Implant Defined Anti-Guided Vertical-Cavity Surface-Emitting Laser Arrays

Dominic F. Siriani, *Student Member, IEEE,* and Kent D. Choquette, *Fellow, IEEE*

***Abstract*— Anti-guided vertical-cavity surface-emitting laser (VCSEL) arrays can be designed to consistently operate in-phase, i.e., with a narrow, on-axis peak in the far field. However, the fabrication of such arrays typically requires anisotropic etching and epitaxial regrowth steps. We have found that anti-guiding behavior can be realized in implant-defined VCSEL arrays. The primary advantage is that the laser arrays can be designed to operate in-phase without requiring any fabrication steps more complicated than those used for conventional implant VCSELs. We present our array structure, a theoretical treatment of the anti-guiding confinement, and experimental results showing the behavior characteristic of anti-guided arrays.**

***Index Terms*— Optical coupling, semiconductor laser arrays, surface-emitting lasers.**

I. Introduction

COHERENTLY coupled laser arrays are useful to create both high-brightness and steerable laser sources, which have potential applications in imaging, sensing, and communications. For these applications, it is desirable to have a single coherent mode that produces an on-axis angularly narrow beam. Vertical-cavity surface-emitting laser (VCSEL) arrays are of interest because of their low cost, high yield, manufacturing ease, and 2-D configurability.

Several means of optical confinement have been used to define VCSEL array elements, including mirror etching [1]–[3] and patterned metal [4]–[6]. However, these array designs typically operate in out-of-phase modes. In recent years, much research attention has been focused on anti-guided (a.k.a. leaky-mode) VCSEL arrays, since they can be designed to consistently operate in an in-phase mode [7]–[9]. The drawback of such arrays is that they require high-fidelity anisotropic etching and epitaxial regrowth steps, which significantly increase the complexity and cost of fabrication.

We recently have reported consistent and reproducible in-phase operation of 2-D implant-defined VCSEL arrays [10], [11]. The laser arrays were found to have very stable modal properties over the full range of operation from threshold to maximum output power. In this paper, we demonstrate that the in-phase operation is primarily a result of index anti-guiding. The anti-guiding effect is very similar to that already described in implanted edge-emitting laser arrays [12]. Since anti-guided arrays couple via leaky modes, design parameters such as element separation are important in determining the dominant array mode. Using a simple thermal and carrier model, the conditions for anti-guiding can be reasonably determined and the dominant mode can be predicted. We show that comparisons between this theory and experiments are in good agreement. Implant-defined anti-guided VCSEL arrays are a considerably simpler and cheaper alternative to other anti-guided array configurations. Due to the importance of anti-guided array technology, these arrays could mark a significant step forward in making practical and economical coherent arrays.

Manuscript received June 10, 2010; revised August 8, 2010; accepted August 11, 2010. Date of current version January 7, 2011. This work was supported in part by the DoD National Defense Science and Engineering Graduate Fellowship.

The authors are with the Department of Electrical and Computer Engineering, University of Illinois at Urbana-Champaign, Urbana, IL 61801 USA (e-mail: siriani@illinois.edu; choquett@illinois.edu).

Color versions of one or more of the figures in this paper are available online at http://ieeexplore.ieee.org.

Digital Object Identifier 10.1109/JQE.2010.2068278

II. Implant Array Structure

The arrays are fabricated in VCSEL epitaxial material designed to operate at 850 nm with 27 p-doped top distributed Bragg reflector (DBR) periods and 35 n-doped bottom DBR periods. Ion implantation is used to electrically define each array element, and a periodic pattern of holes is etched to limit the number of lasing modes and to provide stable index guiding around the outside of the array [11]. Metal is deposited over the entire backside of the wafer and is patterned into ring contacts on the top surface. Using inductively coupled plasma reactive-ion etch and a silicon dioxide mask, the periodic hole pattern is etched into the top DBR. Following the etch step, thick photoresist is used to define the unimplanted regions that constitute the laser array. Proton implantation is performed with the sample at a 7° tilt and a dose and energy of 4×10^{14} cm^{-2} and 340 keV, respectively. Finally, multiple implantations at varying energies are used to provide electrical isolation between different laser arrays. A schematic representation of the laser arrays and an image of a fabricated array are shown in Fig. 1.

The arrays investigated have two elements with varying separations from 9 to 14.5 μm in 0.5-μm steps. The implant apertures are designed to be circular with a radius of 3.5 μm, although it is expected that the actual apertures are smaller than this. Moreover, the elements of an array are designed to be identical, but factors such as misalignment during photolithography steps or nonuniformity in the resist implant mask can cause variations. These variations can result in different aperture sizes, resistances, thresholds, etc., which create asymmetry in the array.

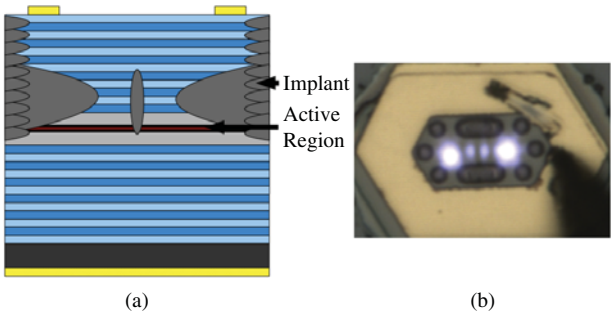

Fig. 1. (a) Cross-section drawing of the implant arrays that are modeled and tested. (b) Top view of a fabricated array while lasing.

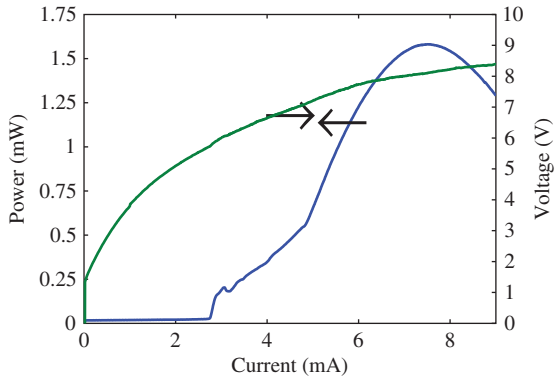

Fig. 2. Laser voltage vs. laser current of a two-element array showing that the power dissipated around threshold is approximately 15 mW.

III. Index Anti-Guiding Analysis

A. Index Model

Coherently coupled VCSEL arrays have been demonstrated using implantation alone [10] as well as with etched holes [11]. Since the focus of this paper is on the dynamics in the coupling region between laser elements (i.e., where there are no etched holes), the effects of the holes are ignored in the theoretical treatment in order to simplify the problem. Thus, the index model we employ incorporates both thermally induced and carrier-induced index shifts superimposed onto a constant index background. Many of the assumptions used are taken from the analysis of thermal effects in VCSELs in [13]. In particular, the medium is assumed to be 2-D (infinite in the longitudinal direction) with conductivity $\sigma = 0.14$ W/cm·K, where the change in index due to carrier concentration N is $\partial n/\partial N = -10^{-21}$ cm^3 and the index change due to temperature T is $\partial n/\partial T = 4 \times 10^{-4}$ K^{-1}. The carrier concentration is modeled as an abrupt step with the same width as the aperture, and the carrier injection is assumed to be $\Delta N = 5 \times 10^{18}$ cm^{-3}. This carrier distribution is justified by the observation of luminescence only inside the implant apertures.

The heat sources are assumed to be Gaussian, i.e., of the form $e^{-(r-r_c)^2/a^2}$ where $r^2 = x^2 + y^2$, r_c is the center of a particular aperture, and a is the aperture radius. The apertures are set to the nominal radius of 3.5 μm. The amount of power dissipated as heat in each aperture is assumed to be around $Q = 7.5$ mW (15 mW total), which is estimated from the current–voltage characteristics above threshold (Fig. 2). All measurements are performed at approximately threshold current. At this current, most power is dissipated as heat, and this dissipated power can readily be estimated using the current–voltage characteristic. It is worth noting that the series resistance is relatively high, which occurs because the electrical contacts are deposited on top of the implanted regions [11]. The power is assumed to be dissipated in a volume of $5\pi a^2$ μm^3 (i.e., 5 μm in the longitudinal direction and the aperture area in the transverse directions). This yields the diffusion equation

$$\frac{\partial^2 T}{\partial x^2} + \frac{\partial^2 T}{\partial y^2} = -\frac{Q}{\sigma}\left(e^{\frac{-(r-r_c)^2}{a^2}} + e^{\frac{-(r+r_c)^2}{a^2}}\right). \quad (1)$$

The diffusion equation is solved numerically using the finite element method. Dirichlet boundary conditions are applied 20 μm away from the four sides of the array. This effectively simulates heat sinking that occurs far from the array elements. Fig. 3 shows a temperature profile found by solving (1). The highest temperature is found in the center of each aperture, with a sharp drop in temperature outside of the array. However, a significant feature is that there is only a very slight drop in temperature between the array elements.

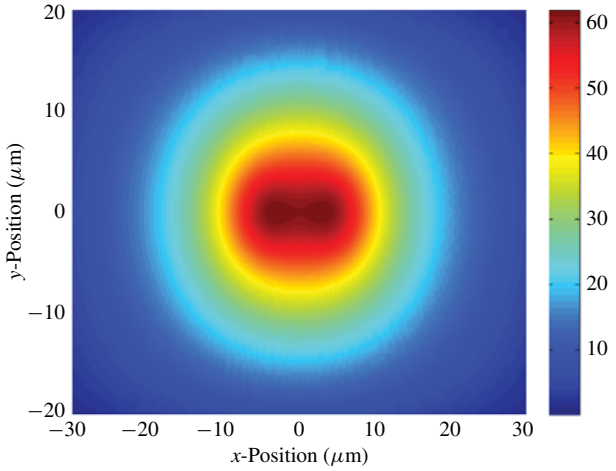

Fig. 3. Temperature profile above ambient temperature in °C for a two-element array.

Using the index parameters given above and assuming a background refractive index of 3.38 at room temperature, the net refractive index profile can be calculated. Fig. 4 shows a calculated index profile that takes into account both thermal and carrier effects. The figure illustrates that the region between the array elements, which is assumed to be subject only to thermal effects, has a higher index than the adjacent aperture regions. The small index shift introduced by the temperature gradient can be overcome by the index shift created by the implant-confined carriers. The net effect is to create a region of anti-guiding in the coupling region with approximate index step Δn_c between the elements, as can be seen in Fig. 4.

Since the index step is dependent on the temperature profile between the implant apertures, it is expected that it will change with both separation and heating. Fig. 5 illustrates the change in the index step at the edge and center of the coupling

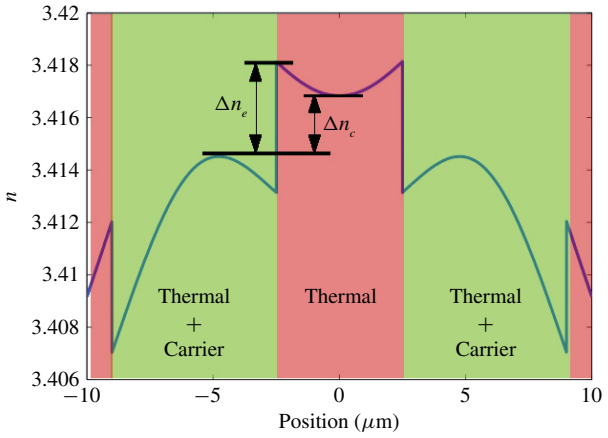

Fig. 4. Calculated index profile for a two-element array along the direction of coupling. The different index regions and the index steps, Δn_e and Δn_c at the edge and center of the coupling region, respectively, are labeled.

region in Fig. 4. It is evident that the index step decreases as both the separation and dissipated power increase, which corresponds to the thermally induced index shift eventually overcoming the carrier-induced shift. Nevertheless, for the chosen parameters, the index anti-guiding condition is met for a wide range of separations and powers. This implies that it is possible to design these anti-guided implant arrays in a variety of configurations and it should be possible to operate them over a wide range of currents.

B. Array Modes and Discrimination

Using the index profiles found via the methods described in the previous section, it is possible to calculate the array modes. The approach used is similar to that in [14]. In particular, a 2-D Helmholtz equation is assumed to be approximately separable so that the problem can be solved for a 1-D cut of the index profile, as illustrated in Fig. 4. The carrier concentration inside each aperture provides material gain, so we assume that this gain perturbs the index with an imaginary part of 0.002. We also assume that the other regions of the array have negligible gain or loss.

We are primarily interested in the gain discrimination between modes. Following the arguments made by Hadley [14], we can reduce the 2-D system to a pair of 1-D problems. Assuming separability and solutions of the form

$$H_{ij}(x, y) = \psi_i(x)\psi_j(y) \tag{2}$$

in the Helmholtz equation

$$\frac{\partial^2 H}{\partial x^2} + \frac{\partial^2 H}{\partial y^2} = k_0^2 \left[\overline{\epsilon} - \epsilon(x, y)\right] H \tag{3}$$

we find the 1-D equation [14]

$$\frac{\partial^2 \psi_i}{\partial x^2} = k_0^2 \left[\overline{\epsilon}_i - \epsilon_r - \Delta\epsilon(x)\right] \psi_i \tag{4}$$

where ψ_i is the mode profile along one direction, k_0 is the free space wavenumber, $\overline{\epsilon}_i$ is the eigenvalue, ϵ_r is the background index, and $\Delta\epsilon(x)$ is the index variation along one direction. If the modes along one direction are identical (in this case, along the direction perpendicular to the coupling), then $\Delta\overline{\epsilon}_j = 0$ and the total modal gain discrimination between the mth and nth modes is equal to that of the other direction, given by

$$\Delta\overline{\epsilon}^{\,2D} = \Delta\overline{\epsilon}_i = \overline{\epsilon}_i^{(m)} - \overline{\epsilon}_i^{(n)}. \tag{5}$$

The 1-D Helmholtz eigenvalue equation (4) is solved using the finite difference approach. The imaginary parts of the eigenvalues are the modal gains, and the eigenvectors give the corresponding mode profiles. The modal gain discrimination for the dominant mode (i.e., the difference in gain for the two modes experiencing the most gain) is calculated as a function of element separation and power dissipated as heat as shown in Fig. 6. As is expected for anti-guided arrays, the dominant mode changes with the inter-element separation due to the change in lateral resonance [15]. Specifically, the number of fringes in between the two major lobes of the mode increases as the separation increases. This is significant because the number of fringes changes the mode between being in-phase and out-of-phase (i.e., one fringe corresponds to in-phase with an on-axis maximum in the far field, two fringes corresponds to out-of-phase with an on-axis null in the far

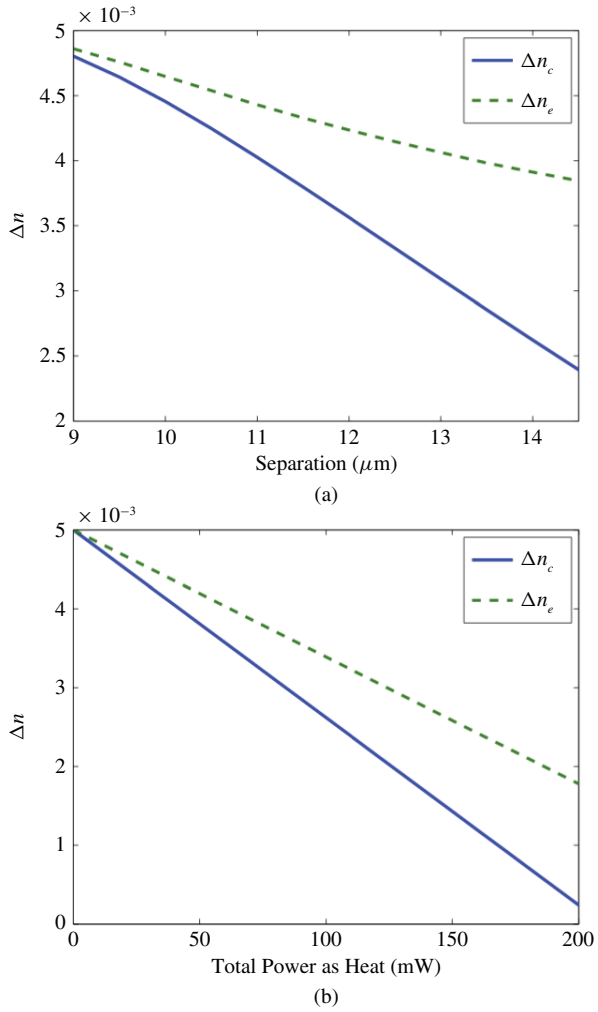

Fig. 5. Calculated index steps (Δn_e and Δn_c as illustrated in Fig. 4) as a function of (a) element separation for 15 mW of heat and (b) power dissipated as heat for a separation of 9.5 μm.

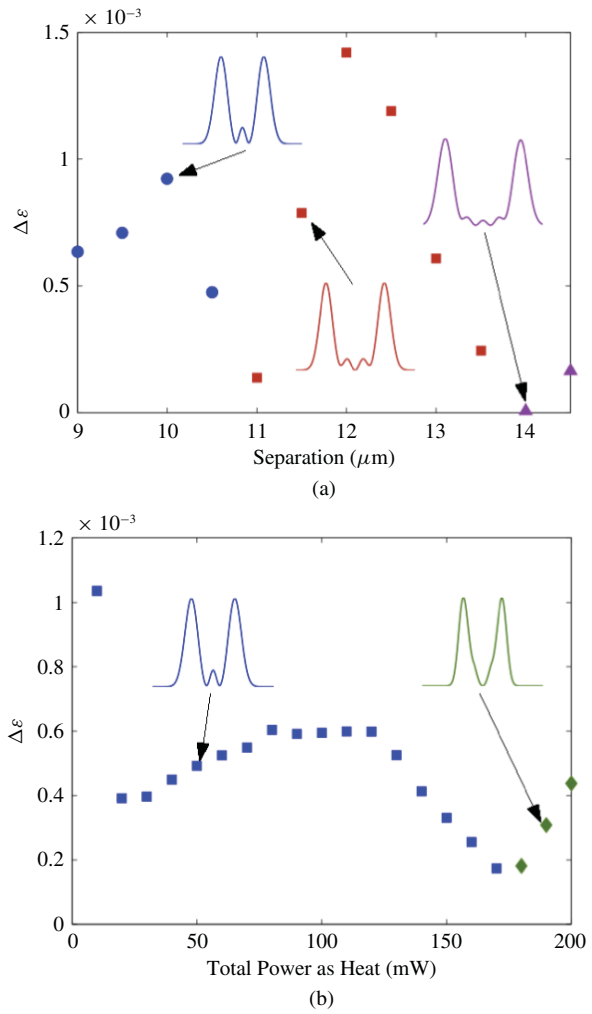

Fig. 6. Calculated modal gain discrimination as a function of (a) element separation for 15 mW of heat and (b) power dissipated as heat for a separation of 9.5 μm. The insets show the dominant mode intensity profile associated with each set of points (i.e., each shape corresponds to the indicated near-field mode profile).

TABLE I
NUMBER OF CENTRAL LOBES

Separation (μm)	Experiment	Theory
9	1	1
9.5	1	1
10	1	1
10.5	-	1
11	2	2
11.5	2	2
12	2	2
12.5	2	2
13	2	2
13.5	2	2
14	2	3
14.5	3	3

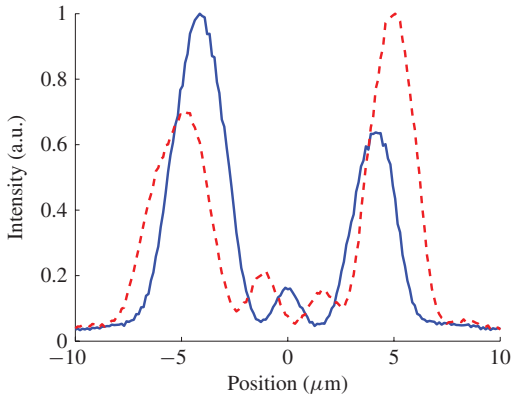

Fig. 7. Measured near-zone modes of two laser arrays with separations of 9 μm (solid) and 11 μm (dashed). The change in the number of central fringes is characteristic of anti-guided arrays.

field, three fringes corresponds to in-phase, etc.). Interestingly, the dominant mode also can change as the power dissipated as heat increases, which again can be attributed to a change to lateral resonance from a change in inter-element index. However, it is evident that this change occurs only for high heating, otherwise the mode is very stable.

IV. EXPERIMENTAL RESULTS

A set of 1 × 2 VCSEL arrays were tested and compared with the results found using the theory of the previous section. These arrays exhibit reproducible modal characteristics over the injection current range from threshold to maximum output power, with a single stable mode lasing at threshold current. A representative light and voltage vs. current characteristic is shown in Fig. 2. The relatively high series resistance arises because the electrical contacts are deposited onto the implanted semiconductor [11]. Measurements were taken at approximately threshold current. In order to verify the anti-guiding hypothesis, the near-field mode profiles of the different VCSEL arrays were measured using a charge coupled device camera. As predicted and previously observed in other anti-guided VCSEL arrays [7], the mode at threshold changes with the separation between the two array elements. The results are summarized in Table I, which shows the number of central lobes between the dominant lobes of the mode profile [see Fig. 1(b)]. The predicted behavior matches closely with the experimental observations. One exception is the 14-μm separation, where three lobes are predicted but only two are observed. Referring to Fig. 6, it is evident that at this separation the modal gain discrimination is very low, so small variations in the assumed parameters could explain the disagreement.

In addition to the good agreement with the behavioral trends, there is also good qualitative agreement between the profiles of the calculated and measured array modes. Fig. 7 shows the two measured modes for separations of 9 and 11 μm. Comparison of these profiles with those in the insets of Fig. 6 reveals that the modes have nearly identical features. In particular, in both cases there are two major lobes that are contained within the implant apertures. Between these lobes, there is either one or two subsidiary lobes that are nearly an order of magnitude lower intensity. For an even number of subsidiary lobes, such as observed with 11-μm separation,

the far field shows an out-of-phase profile, while for an odd number of lobes, such as observed with 9 μm, an in-phase far-field pattern is observed.

V. Conclusion

We have demonstrated a novel anti-guiding VCSEL array that has significant fabrication advantages over previous approaches due to its simplicity and low cost. A theoretical model has been presented that illustrates the origin of index anti-guiding. Moreover, the model demonstrates that the anti-guiding can be stable for a variety of designs and over a wide range of operating conditions. Experimental evidence agrees well with the theoretical treatment and serves to verify the anti-guiding hypothesis. It is also demonstrated that careful design must be carried out in order to maintain single-mode operation. The design of anti-guiding in implant arrays is significant for the pursuit of low-cost high-power VCSEL arrays. In future work, we will address scaling to larger array sizes (greater than 2×2) for higher output powers.

Acknowledgment

The authors would like to thank A. Danner and Avago Technologies, San Jose, CA, for epitaxial wafers.

References

[1] H. Yoo, A. Scherer, J. Harbison, L. Florez, E. Paek, B. van der Gaag, J. Hayes, A. von Lehmen, E. Kapon, and Y. Kwon, "Fabrication of a 2-D phased array of vertical-cavity surface-emitting lasers," *Appl. Phys. Lett.*, vol. 56, no. 13, pp. 1198–1200, 1990.

[2] P. L. Gourley, M. E. Warren, G. R. Hadley, G. A. Vawter, T. M. Brennan, and B. E. Hammons, "Coherent beams from high efficiency 2-D surface-emitting semiconductor laser arrays," *Appl. Phys. Lett.*, vol. 58, no. 9, pp. 890–892, Mar. 1991.

[3] A. J. Danner, J. C. Lee, J. J. Raftery, Jr., N. Yokouchi, and K. D. Choquette, "Coupled-defect photonic crystal vertical cavity surface emitting lasers," *Electron. Lett.*, vol. 39, no. 18, pp. 1323–1324, Sep. 2003.

[4] M. Orenstein, E. Kapon, N. G. Stoffel, J. P. Harbison, L. T. Florez, and J. Wullert, "2-D phase-locked arrays of vertical-cavity semiconductor lasers by mirror reflectivity modulation," *Appl. Phys. Lett.*, vol. 58, no. 8, pp. 804–806, Feb. 1991.

[5] R. A. Morgan, K. Kojima, T. Mullally, G. D. Guth, M. W. Focht, R. E. Leibenguth, and M. Asom, "High-power coherently coupled 8×8 vertical cavity surface emitting laser array," *Appl. Phys. Lett.*, vol. 61, no. 10, pp. 1160–1162, Sep. 1992.

[6] F. M. di Sopra, M. Brunner, H.-P. Gauggel, H. P. Zappe, M. Moser, R. Hövel, and E. Kapon, "Continuous-wave operation of phase-coupled vertical-cavity surface-emitting laser arrays," *Appl. Phys. Lett.*, vol. 77, no. 15, pp. 2283–2285, Oct. 2000.

[7] D. K. Serkland, K. D. Choquette, G. R. Hadley, K. M. Geib, and A. A. Allerman, "Two-element phased array of antiguided vertical-cavity lasers," *Appl. Phys. Lett.*, vol. 75, no. 24, pp. 3754–3756, Dec. 1999.

[8] D. Zhou, L. J. Mawst, and Z. Dai, "Modal properties of 2-D antiguided vertical-cavity surface-emitting laser arrays," *IEEE J. Quantum Electron.*, vol. 38, no. 6, pp. 652–664, Jun. 2002.

[9] L. Bao, N.-H. Kim, L. J. Mawst, N. N. Elkin, V. N. Troshchieva, D. V. Vysotsky, and A. P. Napartovich, "Near-diffraction-limited coherent emission from large aperture antiguided vertical-cavity surface-emitting laser arrays," *Appl. Phys. Lett.*, vol. 84, no. 3, pp. 320–322, Jan. 2004.

[10] A. C. Lehman and K. D. Choquette, "1- and 2-D coherently coupled implant-defined vertical-cavity laser arrays," *IEEE Photon. Technol. Lett.*, vol. 19, no. 19, pp. 1421–1423, Oct. 2007.

[11] D. F. Siriani and K. D. Choquette, "In-phase, coherent photonic crystal vertical-cavity surface-emitting laser arrays with low divergence," *Electron. Lett.*, vol. 46, no. 10, pp. 712–714, May 2010.

[12] E. Kapon, C. Lindsey, S. Margalit, A. Yariv, and J. Katz, "Coupling mechanism of gain-guided integrated semiconductor laser arrays," *Appl. Phys. Lett.*, vol. 44, no. 4, pp. 389–391, Feb. 1984.

[13] N. K. Dutta, L. W. Tu, G. Hasnain, G. Zydzik, Y. H. Wang, and A. Y. Cho, "Anomalous temporal response of gain guided surface emitting lasers," *Electron. Lett.*, vol. 27, no. 3, pp. 208–210, Jan. 1991.

[14] G. R. Hadley, "Modes of a 2-D phase-locked array of vertical-cavity surface-emitting lasers," *Opt. Lett.*, vol. 15, no. 21, pp. 1215–1217, 1990.

[15] D. Botez and L. J. Mawst, "Phase-locked laser arrays revisited," *IEEE Circuits Devices Mag.*, vol. 12, no. 6, pp. 25–32, Nov. 1996.

Dominic F. Siriani (S'07) received the B.S. and M.S. degrees in electrical engineering from the University of Illinois at Urbana-Champaign, Urbana, in 2006 and 2007, respectively, and is currently pursuing the Ph.D. degree at the same university.

His current research interests include photonic crystal vertical-cavity surface-emitting lasers (VCSELs), VCSEL arrays, beam combining and beam steering, coupled mode theory, and coherence theory.

Mr. Siriani is a Student Member of the IEEE Photonics Society, a National Science Foundation Graduate Fellow, and a National Defense Science and Engineering Graduate Fellow.

Kent D. Choquette (M'97–F'03) received the B.S. degree in engineering physics and applied mathematics from the University of Colorado, Boulder, and the M.S. and Ph.D. degrees in materials science from the University of Wisconsin-Madison, Madison.

He was with Sandia National Laboratories, Albuquerque, NM, after a post-doctoral appointment at AT&T Bell Laboratories, Murray Hill, NJ. Since 2000, he has been a Professor in the Department of Electrical and Computer Engineering, University of Illinois at Urbana-Champaign, Urbana. He has authored more than 200 publications and three book chapters, and has presented numerous invited talks and tutorials. His current research interests include the design, fabrication, characterization, and applications of vertical-cavity surface-emitting lasers, photonic crystal light sources, nanofabrication technologies, and hybrid integration techniques for photonic devices.

Dr. Choquette is a Fellow of the Optical Society of America and the Society of Photo-Optical Instrumentation Engineers. He was awarded the 2008 IEEE/Lasers and Electro-Optical Society Engineering Achievement Award. He has served as an Associate Editor of the IEEE Journal of Quantum Electronics, IEEE Photonic Technology Letters, and *Journal of Lightwave Technology*, as well as a Guest Editor of the IEEE Journal of Selected Topics in Quantum Electronics.